Stem Cell Reports
Article

ISSCR

OPEN ACCESS

DOT1L regulates lung developmental epithelial cell fate and adult alveolar stem cell differentiation after acute injury

Shanru Li,[1,2] Derek Liberti,[1,2] Su Zhou,[1,2] Yun Ying,[1,2] Jun Kong,[1,2] Maria C. Basil,[1,2] Fabian L. Cardenas-Diaz,[1,2] Kazushige Shiraishi,[1,2] Michael P. Morley,[1,2] and Edward E. Morrisey[1,2,3,*]

[1]Department of Medicine, Perelman School of Medicine, University of Pennsylvania, Philadelphia, PA 19104, USA
[2]Penn-CHOP Lung Biology Institute, Perelman School of Medicine, University of Pennsylvania, Philadelphia, PA 19104, USA
[3]Department of Cell and Developmental Biology, Perelman School of Medicine, University of Pennsylvania, Philadelphia, PA 19104, USA
*Correspondence: emorrise@pennmedicine.upenn.edu
https://doi.org/10.1016/j.stemcr.2023.07.006

SUMMARY

AT2 cells harbor alveolar stem cell activity in the lung and can self-renew and differentiate into AT1 cells during homeostasis and after injury. To identify epigenetic pathways that control the AT2-AT1 regenerative response in the lung, we performed an organoid screen using a library of pharmacological epigenetic inhibitors. This screen identified DOT1L as a regulator of AT2 cell growth and differentiation. *In vivo* inactivation of *Dot1l* leads to precocious activation of both AT1 and AT2 gene expression during lung development and accelerated AT1 cell differentiation after acute lung injury. Single-cell transcriptome analysis reveals the presence of a new AT2 cell state upon loss of *Dot1l*, characterized by increased expression of oxidative phosphorylation genes and changes in expression of critical transcription and epigenetic factors. Taken together, these data demonstrate that *Dot1l* controls the rate of alveolar epithelial cell fate acquisition during development and regeneration after acute injury.

INTRODUCTION

The lung alveolus is the primary site of gas exchange between the circulatory system and the external environment in mammals. The alveolus is comprised of multifarious epithelial, mesenchymal, endothelial, and immune lineages, all of which communicate with each other in a complex and plastic manner during development, adult homeostasis, and after injury (reviewed in Basil et al., 2020; Zepp and Morrisey 2019; Leach and Morrisey 2018). Alveolar type 1 (AT1) and alveolar type 2 (AT2) are the two primary epithelial cell lineages within the lung alveolus. AT1 cells are responsible for forming the thin gas-diffusible interface with the endothelial plexus and AT2 cells are responsible for generating and regulating pulmonary surfactant. AT2 cells can also act as facultative progenitors after lung injury in part through a Wnt responsive subpopulation called alveolar epithelial progenitors (Zacharias et al., 2018; Nabhan et al., 2018), which can proliferate and differentiate to replenish the alveolar epithelium. The balance between AT2 cell proliferation and differentiation into AT1 cells is crucial for maintaining normal alveolar structure and function and proper gas exchange during homeostasis and after injury.

Several signal transduction pathways control AT2 cell proliferation and differentiation into AT1 cells. For instance, Wnt signaling has been shown to promote AT2 cell lineage commitment and proliferation and to inhibit differentiation into AT1 cells (Zacharias et al., 2018; Nabhan et al., 2018; Frank et al., 2016; Li et al., 2018; Liberti et al., 2021). Epigenetic factors have also been shown to play important roles in lung epithelial development. *Hdac1/2* are critical regulators of proximal airway development, whereas *Hdac3* plays a key role in AT1 cell development through regulation of TGF-β signaling (Wang et al. 2013, 2016a, 2016b). In contrast, *Dnmt1* suppresses precocious AT2 cell fate commitment (Liberti et al., 2019). Despite these insights, less is known about the role of epigenetic factors in the complex regenerative process that occurs after an acute injury in the lung.

To identify epigenetic pathways that regulate the response of lung alveolar epithelial cells to injury, we performed a mouse alveolar organoid screen using a library of pharmacological epigenetic inhibitors. These studies identified multiple inhibitors of disrupter of telomeric silencing 1-like (DOT1L), a histone H3K79 methyltransferase, that increased alveolar organoid size. Addition of DOT1L inhibitors increased expression of both AT1 and AT2 marker genes in alveolar organoids. To explore the role of *Dot1l* during lung development and regeneration, we generated a *Dot1l* conditional knockout allele and showed that genetic loss of *Dot1l* also leads to increased alveolar organoid size. Loss of *Dot1l* during lung endoderm development led to precocious and increased AT1 and AT2 cell fate specification as noted by expression of cell-type-specific marker genes prior to their normal onset of expression. In two adult acute lung injury models, *Dot1l*-deficient AT2 cells exhibited an accelerated rate of AT1 cell differentiation without changing the rate of epithelial cell proliferation. Single-cell RNA-seq (scRNA-seq) analysis of *Dot1l*-deficient lineage-traced AT2 cells reveals the emergence of a new subset of AT2 cells characterized by increased expression of a host of oxidative phosphorylation (OxPhos) metabolism genes and several important

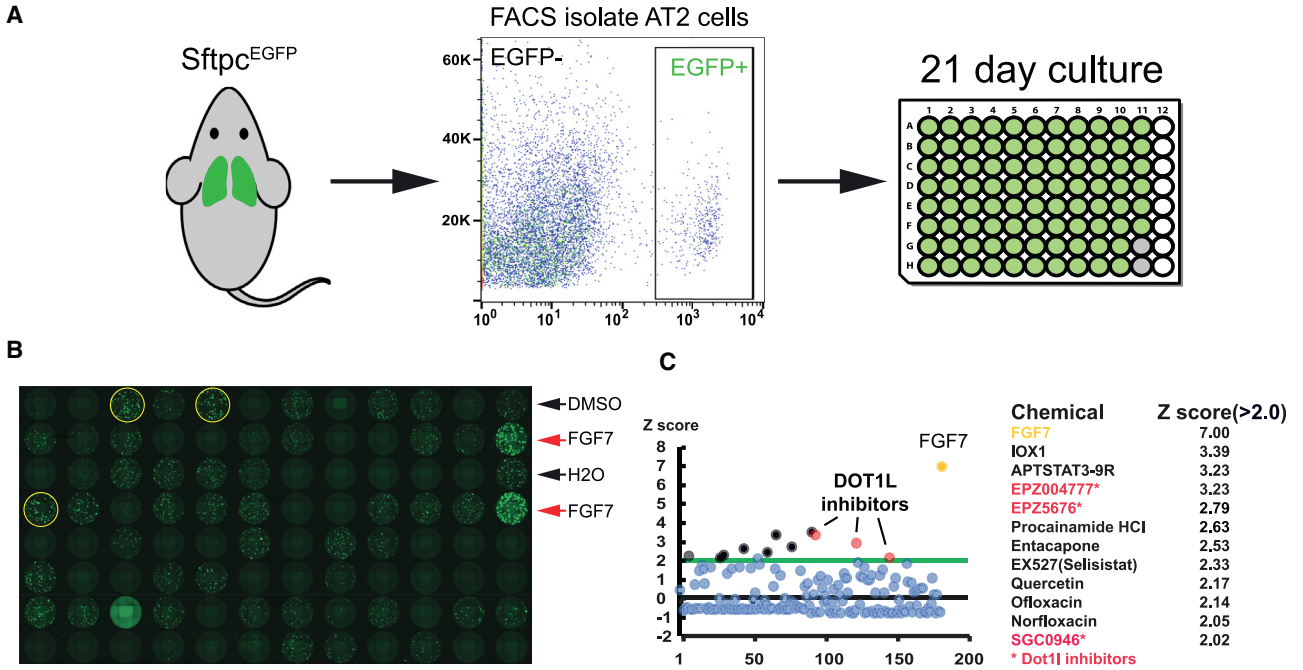

Figure 1. Alveolar organoid screen to identify epigenetic pathways regulating alveolar regeneration

(A) Schematic of how AT2 cells isolated from *Sftpc*^{EGFP} mice were used in the screen.

(B) An example of fluorescent reporter detection from *Sftpc*^{EGFP} AT2 cells in a 96-well plate. Arrows indicate negative (water or DMSO) or positive (FGF7) controls used for the screen.

(C) Results from the epigenetic small molecular inhibitor library using a *Z* score of 2.0 as a cutoff for a positive increase in alveolar organoid total fluorescence. Data are representative of the screening assay performed in duplicate.

transcriptional and epigenetic regulators of lung development including *Id1* and *Id2*. These data highlight the importance of *Dot1l* in restraining AT2-AT1 differentiation while not affecting cellular proliferation after acute lung injury.

RESULTS

Small-molecule screen identifies inhibitors of DOT1L that increase lung alveolar organoid size

To identify and characterize epigenetic pathways that regulate lung alveolar regeneration, we established a medium throughout organoid screen in 96-well plates. We utilized a minimal medium that lacked ROCK and TGF-β inhibitors, as the presence of these factors may negate the effects of additional factors from the library and confound the results. Mouse AT2 cells were FACS isolated from *Sftpc*^{EGFP} mice and plated along with primary mouse lung fibroblasts in a Matrigel-based culture medium. Forty-eight hours after plating, a library of pharmacological epigenetic inhibitors representing many of the major epigenetic pathways was added to the medium and the organoids were cultured for an additional 19 days (Figure 1A). Total fluorescent intensity, a surrogate for organoid size, was measured throughout the three-dimensional Matrigel culture (Figure 1B). Many epigenetic inhibitors suppressed organoid growth including inhibitors for HDACs and BRD4, both of which are known to be important for cell proliferation (Zhu et al., 2022; Pang et al., 2022; Hu et al., 2022; Sun et al., 2021; Xiang et al., 2018; Nishiyama et al., 2006). In contrast, only a minority of inhibitors caused an increase in organoid size of more than 50% including three known DOT1L inhibitors (Figures 1C; Table S1).

To test whether the DOT1L inhibitors increased alveolar organoid size in a dose-dependent manner, each of the inhibitors was added in a range spanning 0.1–50 μM based on previously described dose ranges for each inhibitor (Daigle et al. 2011, 2013; Yu et al., 2012). As expected, the organoids exhibited different sensitivities to each of the inhibitors, but all revealed a dose-dependent increase in organoid size in ranges that were tested (Figure 2A). Quantitative PCR (qPCR) was used to assess AT1 and AT2 marker gene expression and these results showed increases in AT1 (*Hopx* and *Aqp5*) and AT2 (*Sftpc*) cell gene expression (Figure 2B). Immunohistochemistry (IHC) also demonstrated increased At1 and AT2 cells in DOT1L inhibitor-treated organoids (Figure 2C). These data suggest that inhibition of DOT1L

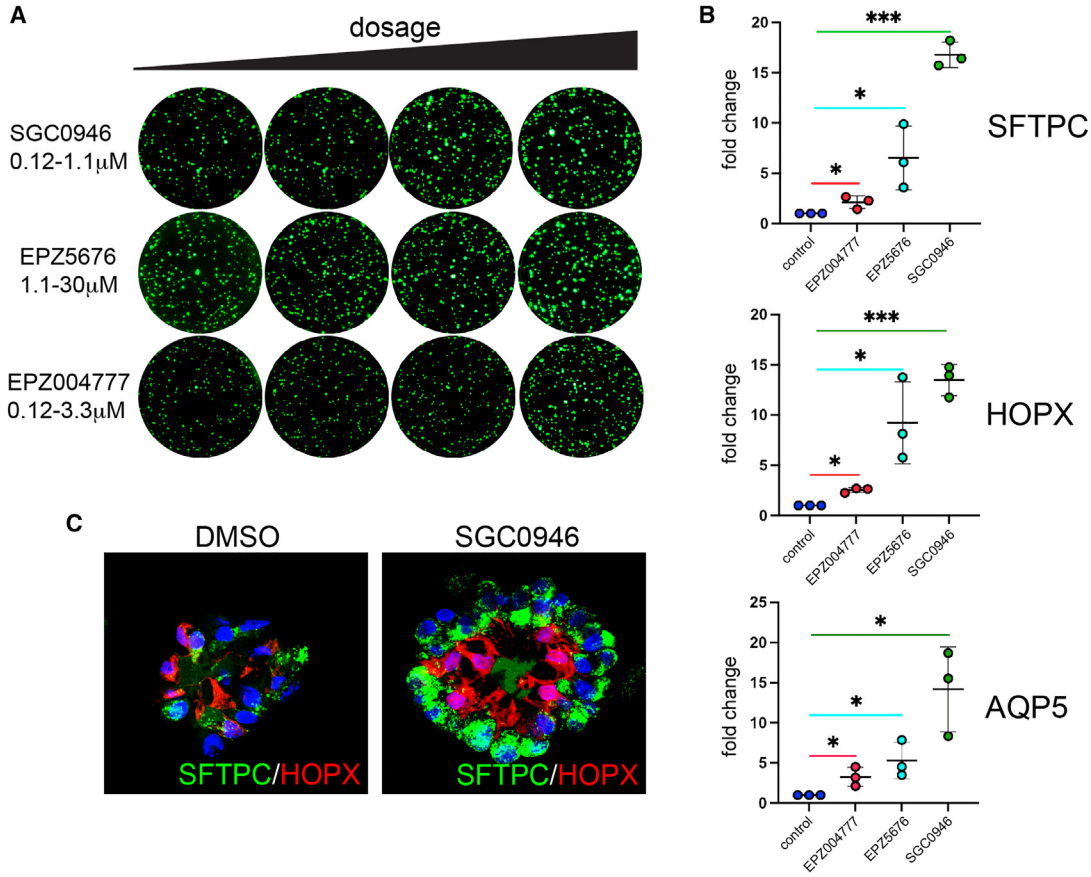

Figure 2. Verification of increased organoid size and AT1 and AT2 cell gene expression by inhibitors of DOT1L

(A) Dose-dependent responses of three of the DOT1L inhibitors on alveolar organoid size. Note, the three inhibitors have different ranges of effective doses, which were covered in the organoid assays shown.

(B) qPCR analysis of AT1 and AT2 cell marker genes in organoids treated with the three DOT1L inhibitors identified in the screen.

(C) IHC of organoids from control and SCG0946 treated showing enhanced expression of *Sftpc* and *Hopx*.

Data represent the average of three separate organoid assays. *p < 0.05, ***p < 0.001.

can increase AT1 and AT2 cell growth and differentiation in organoid assays.

Dot1l is widely expressed in the lung and genetic inactivation in AT2 cells leads to increased alveolar organoid growth

Dot1l expression and the H3K79me2 mark was assessed using IHC in both the developing lung and in adult AT1 and AT2 cells. *Dot1l* expression is widespread during embryonic development in both the developing endoderm and in the surrounding mesenchyme (Figure 3A). The H3K79me2 mark is present in adult AT1 and AT2 cells, indicating DOT1L activity (Figure 3B).

To interrogate the role of *Dot1l* in lung epithelial biology further, we generated a *Dot1l* floxed allele and inactivated *Dot1l* in adult AT2 cells using the $Sftpc^{cre/ERT2}$ line (Figure 3D) (Chapman et al., 2011). Loss of *Dot1l* leads to loss of the H3K79me2 mark in adult AT2 cells (Figure 3E). Moreover, loss of *Dot1l* in adult AT2 cells leads to increased organoid size, similar to that observed using pharmacological inhibitors of DOT11 (Figures 3F and 3G). These data indicate that the increased organoid size observed upon pharmacological inhibition or genetic loss of *Dot1l* expression is an AT2 cell intrinsic response.

Dot1l restrains AT1 and AT2 cell fate acquisition during lung endoderm development

To determine the effects of loss of *Dot1l* on lung endoderm development, we assessed the loss of *Dot1l* expression in the developing lung endoderm using the Shh^{cre} line (Harfe et al., 2004). Loss of H3K79me2 marks was confirmed in the developing lung endoderm and not surrounding mesenchyme by IHC at E15.5 (Figure 4A). Shh^{cre}:$Dot1l^{flox/flox}$ mice (from hereon called $Dot1l^{Shh\text{-}KO}$) were

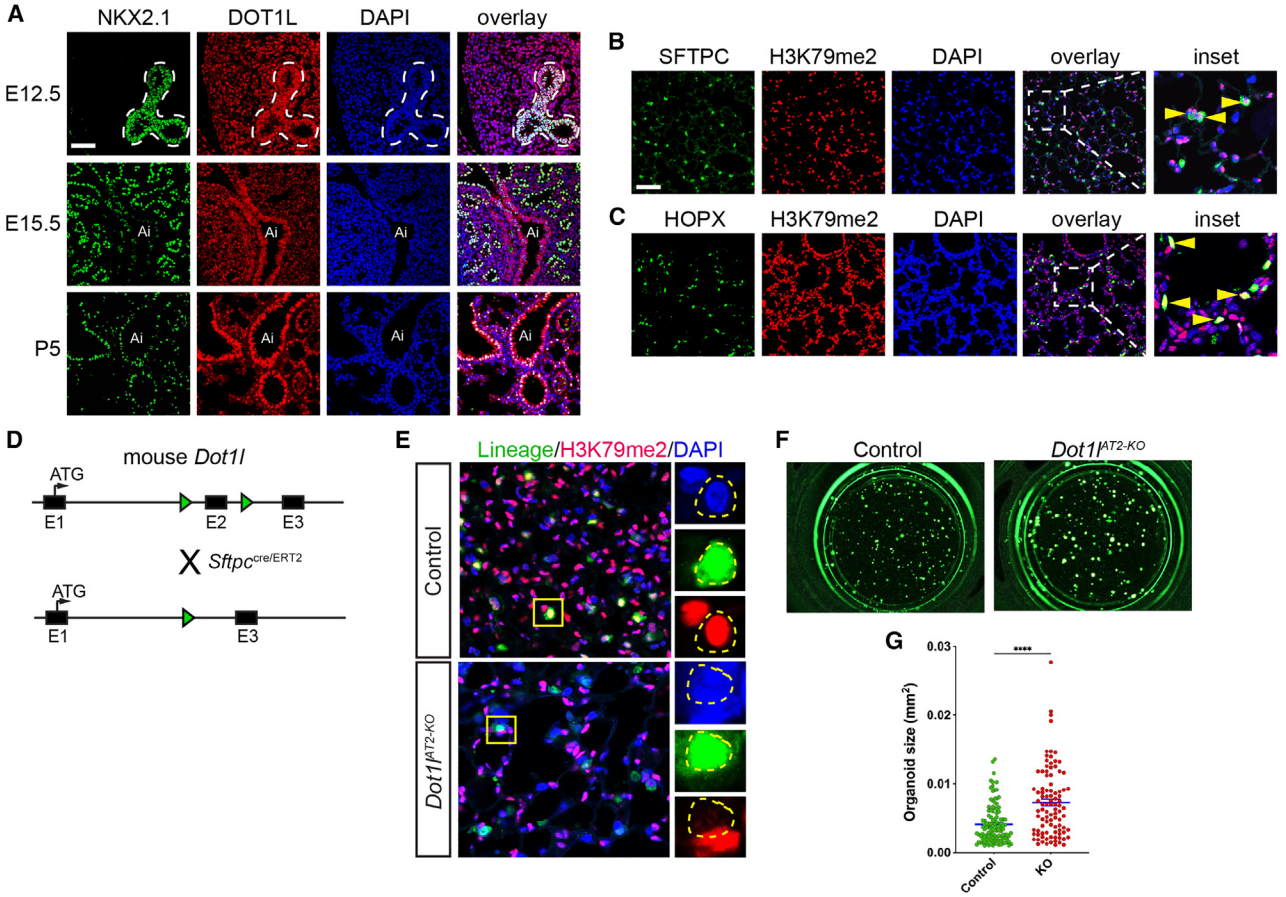

Figure 3. *Dot1l* is broadly expressed in developing and adult lung epithelium and genetic loss leads to increased alveolar organoid size

(A) *Dot1l* expression as assessed by IHC at different time points of mouse lung development. Note high level of expression in lung endoderm.

(B) Expression of the *Dot1l*-mediated histone mark H3K79me2 in adult AT2 cells. Co-expression of *Sftpc* and H3K79me2 are noted by yellow arrows.

(C) Expression of the *Dot1l*-mediated histone mark H3K79me2 in adult AT1 cells. Co-expression of *Hopx* and H3K79me2 are noted by yellow arrowheads.

(D) Schematic of floxed Dot1l allele.

(E) Loss of *Dot1l* in AT2 cells leads to loss of the H3K79me2 mark.

(F) AT2 cells isolated from $Dot1l^{AT2\text{-}KO}$ mutants exhibit increased organoid growth compared with control AT2 cells.

(G) Quantitation of data presented in (E) with n = 3 separate organoid assays. Scale bar, 50 μm. Ai, airway. ****p < 0.0001.

born live without obvious lung structural defects and with no change in AT1-AT2 cell ratios (Figure S1). $Dot1l^{Shh\text{-}KO}$ and littermate controls were examined by RNAscope, IHC and qPCR at various time points during development. As early as E12.5, $Dot1l^{Shh\text{-}KO}$ lungs expressed increased levels of *Sftpc* and *Hopx* (Figure 4B). This is several days earlier than prior reports for the onset of *Hopx* expression (Yin et al., 2006), and prior to full specification of AT1 or AT2 cells (Frank et al., 2019). This increased expression of *Hopx* and *Sftpc* was also observed at E15.5 (Figures 4C and 4D). However, by E17.5 no detectable difference was observed in *Sftpc* and *Hopx* expression (Figure 4C). Thus, *Dot1l* suppresses the rate, rather than overall extent, of AT1 and AT2 cell fate acquisition and gene expression during early lung endoderm.

Loss of *Dot1l* in adult AT2 cells accelerates AT2-AT1 differentiation after acute lung injury

To determine whether *Dot1l* regulated AT2-AT1 cell differentiation after acute lung injury, we performed influenza A (H1N1, PR8) infection and hyperoxic lung injury studies on $Sftpc^{cre/ERT2}$:$Dot1l^{flox/flox}$ mice (from hereon called

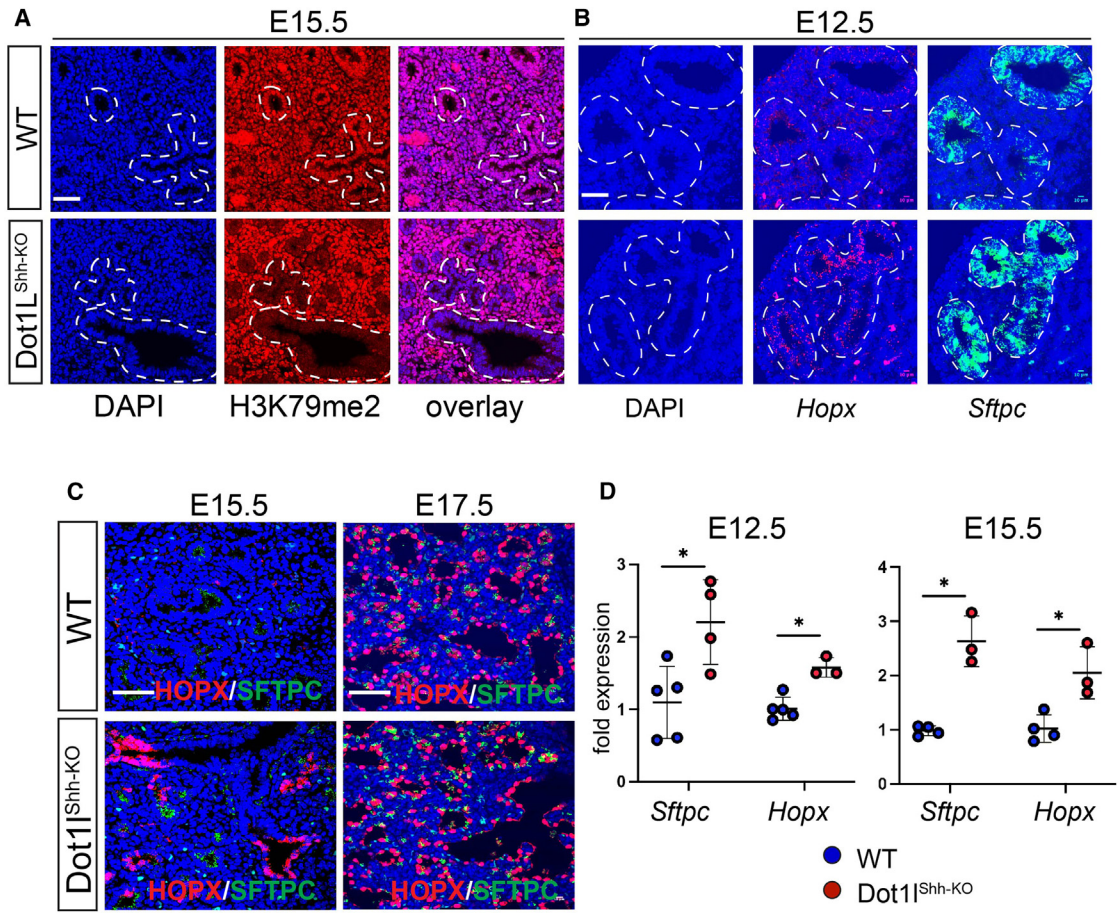

Figure 4. Loss of *Dot1l* during lung endoderm development leads to precocious activation of AT1 and AT2 cell fate and gene expression

(A) Expression of the histone mark H3K79me2 using IHC at E15.5 of mouse lung development. Dotted lines outline airways.

(B) Expression of *Hopx* and *Sftpc* using RNAscope at E12.5 of lung development. Dotted lines outline airways.

(C) Expression of *Hopx* and *Sftpc* at E15.5 and E17.5 using IHC.

(D) qPCR to detect expression of *Hopx* and *Sftpc* at E12.5 and E15.5 of lung development (n = 3–5 separate animals). Scale bar, 50 μm. *p < 0.05.

Dot1l$^{AT2\text{-}KO}$). Animals were collected at times when AT2 cells are known to both be proliferating as well as differentiating into AT1 cells (Figures 5A and 5D). *Dot1l*-deficient AT2 cells exhibited increased AT1 cell differentiation 14 days after influenza infection and 7 days after hyperoxic lung injury in previously defined damaged areas (Figures 5B, 5C, 5E, and 5F) (Liberti et al. 2021, 2022). In contrast, there was no notable difference in AT2 cell proliferation in either of these models (Figure S2). Thus, loss of *Dot1l* increases AT2-AT1 cell differentiation after acute lung injury without affecting cell proliferation.

Dot1l has been reported to play an important role in the DNA damage response (Wood et al. 2018). To assess the degree of DNA damage and repair in control and *Dot1l*$^{AT2\text{-}KO}$ mutant cells, we performed gama-H2AX immunostaining after the injury. There were only rare gama-H2AX-positive cells in both control and *Dot1l*$^{AT2\text{-}KO}$ mutants, suggesting that loss of *Dot1l* in AT2 cells does not affect the DNA damage repair response (Figure S3).

Loss of *Dot1l* leads to the emergence of a metabolically altered AT2 cell state after injury

To assess the cellular and molecular changes that occur in *Dot1l*-deficient alveolar epithelium after acute injury, we performed scRNA-seq analysis on lineage-traced AT2 cells after influenza injury from both control and *Dot1l*$^{AT2\text{-}KO}$ mutants. These two datasets were merged to assess whether there were any new cellular states that occurred due to *Dot1l* deficiency. This analysis identified a cluster of AT2 cells that we called AT2b, which was found almost exclusively in *Dot1l*$^{AT2\text{-}KO}$ mutants (Figures 5F and 5G). AT2b cells expressed AT2 marker genes in a similar manner as control AT2 cells. AT2b cells also expressed higher levels of some

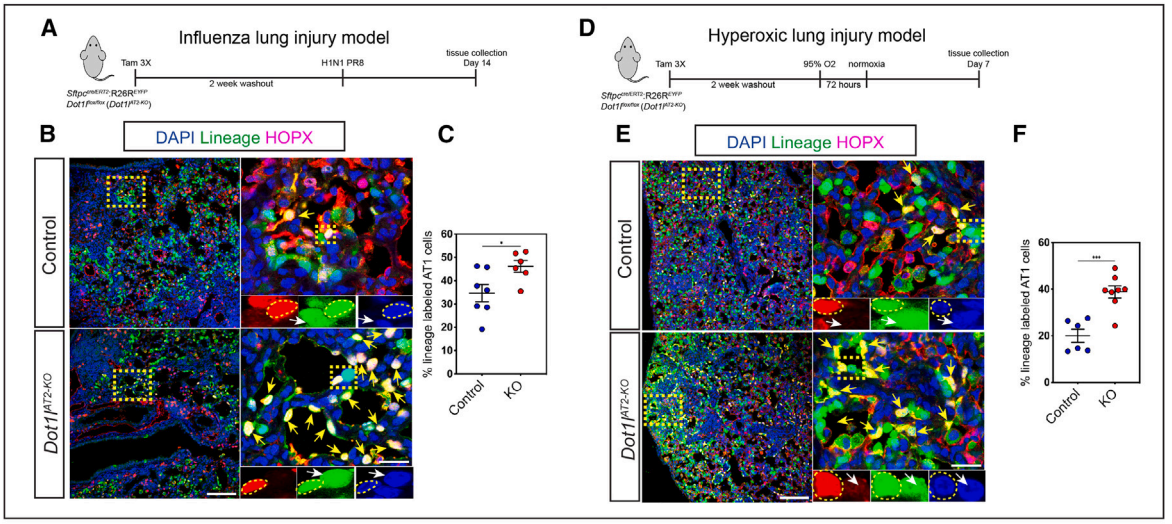

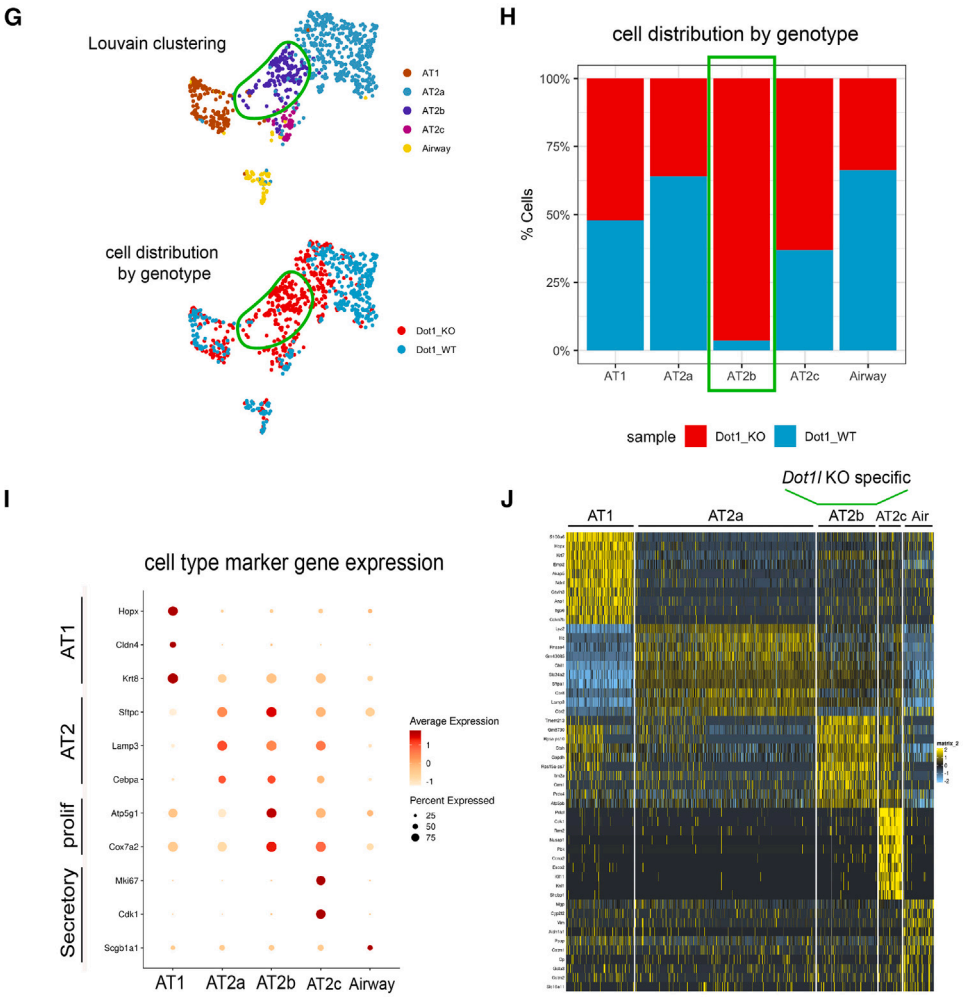

(legend on next page)

AT1 markers, such as *Ager* and *Aqp5*, but did not express genes representing the previously described transition state found as AT2 cells differentiated into AT1 cells (Table S2; Figures 5H, 5I, and S4) (Strunz et al., 2020; Kobayashi et al., 2020; Choi et al., 2020). This suggested that loss of *Dot1l* leads to a new AT2 cell state characterized by increased AT1 marker gene expression. Genes that were increased in the AT2b state were expressed at a fairly high level, with most being expressed in the third and fourth quartile of gene expression (Figure S4). Moreover, we observed a proliferative AT2 cell state, AT2c, that was equally shared between control and $Dot1l^{AT2\text{-}KO}$ mutants (Figures 5F and 5G), supporting the lack of altered proliferation upon loss of *Dot1l*.

Analysis of the genes defining the AT2b cluster identified many genes with the mitochondrial OxPhos pathway (Figure 6A). Examination of the scRNA-seq data shows that there was no significant difference in mitochondrial reads, UMI counts, or total genes counted between control and $Dot1l^{AT2\text{-}KO}$ mutant cells (Figure S5). Gene ontology analysis revealed a high enrichment of several categories related to OxPhos metabolism in the AT2b cluster (Figure S5). Comparison of the top enriched genes in OxPhos across all of the identified epithelial cell types in the scRNA-seq data demonstrated that this pathway was enriched at the highest level in the AT2b cluster but was also elevated in proliferating AT2 cells (AT2c) and in AT1 cells in comparison with resting AT2 cells (AT2a) (Figures 6B and 6C). Pseudotime trajectory analysis suggests that the AT2a cell state transitions through the AT2b state before differentiating into AT1 cells (Figure 6D). Analysis of the gene signature driving this transition shows that the OxPhos genes that characterize the AT2b state are expressed at lower levels during control AT2-AT1 cell differentiation (Figure 6E). In addition to genes in the OxPhos pathway, expression of several important transcription and epigenetic factors was also increased or decreased within the AT2b cell subset (Figure S6). These included the Bmp signaling downstream effectors Id1 and Id2. Previous work has shown that Bmp signaling can promote AT2-AT1 cell differentiation in lung pneumonectomy models of lung regrowth (Chung et al., 2018). These data suggest that *Dot1l* normally restricts a core set of OxPhos metabolomic genes and inhibition of *Dot1l* leads to increased AT2-AT1 differentiation.

To further assess what molecular pathways could be altered in *Dot1l*-deficient AT2 cells leading to increased OxPhos metabolism, we performed single-cell ATAC sequencing (scATAC-seq) analysis at the same time point as we performed scRNA-seq analysis. Comparison of control versus $Dot1l^{AT2\text{-}KO}$ mutant lineage-traced cells shows that both AT1 and AT2 cells were resolved with scATAC-seq (Figure 6F). We also performed CUT&RUN analysis for H3K79me2 marks in AT2 cells. We next filtered on genes that (1) contained H3K79me2 marks, (2) in which expression was downregulated in $Dot1l^{AT2\text{-}KO}$ mutants, and (3) in which scATAC-seq peaks were diminished in $Dot1l^{AT2\text{-}KO}$ mutants (Figure 6G). This resulted in 16 genes that fit all three criteria listed above. A previous study demonstrated that increased expression of fructose-bisphosphatase 2 (Fbp2) leads to decreased activity of OxPhos metabolism (Huangyang et al., 2020; Osipova et al., 2023). Interestingly, Fbp2 gene score by scATAC-seq was decreased in $Dot1l^{AT2\text{-}KO}$ mutants and H3K79me2 marks were found in the Fbp2 promoter region in AT2 cells (Figures 6H and 6I). Thus, decreased Fbp2 expression may explain the elevated levels of OxPhos pathway genes upon loss of Dot1l in AT2 cells. Taken together, Dot1l alters OxPhos metabolism and transcription factor expression that normally restricts AT2-AT1 differentiation and lung alveolar regeneration (Figure 7).

DISCUSSION

Differentiation of AT2 cells into AT1 cells is a cardinal feature of adult lung alveolar regeneration. Promotion of

Figure 5. Loss of *Dot1l* in adult AT2 cells leads to increased AT2-AT1 differentiation and the emergence of a new AT2 cell state after acute lung injury

(A) Schematic of influenza lung injury model.

(B) IHC of control and $Dot1l^{AT2\text{-}KO}$ mutants 14 days after influenza injury. The dashed yellow box indicates the region shown in the insert at the right. Yellow arrows and dashed yellow circles indicate AT2 cell-derived AT1 cells and white arrows mark AT2 cells.

(C) Quantitation of increased AT2-AT1 differentiation in $Dot1l^{AT2\text{-}KO}$ mutants after influenza injury (n = 6–7 animals).

(D) Schematic of hyperoxic lung injury model.

(E) IHC of control and $Dot1l^{AT2\text{-}KO}$ mutants 7 days after hyperoxic lung injury.

(F) Quantitation of increased AT2-AT1 differentiation in $Dot1l^{AT2\text{-}KO}$ mutants after hyperoxic lung injury (n = 6–8 animals).

(G) Louvain clustering and UMAP presentation of the five different clusters of AT2 and AT1 cells lineage-traced cells merged from control and $Dot1l^{AT2\text{-}KO}$ mutants.

(H) Bar graph showing cell distribution by genotype with the AT2b cluster being unique to the *Dot1l* mutants.

(I) Dot plot showing expression of hallmark cell-type-specific marker genes. Note that the AT2b cluster expresses hallmark marker genes of the AT2 lineage.

(J) Heatmap showing the distinct expression pattern of all five clusters of lineage-traced cells in the merged dataset. The *Dot1l* mutant-specific AT2b cluster is highlighted by green brackets. Scale bar, 50 μm. *$p < 0.05$, ***$p < 0.001$.

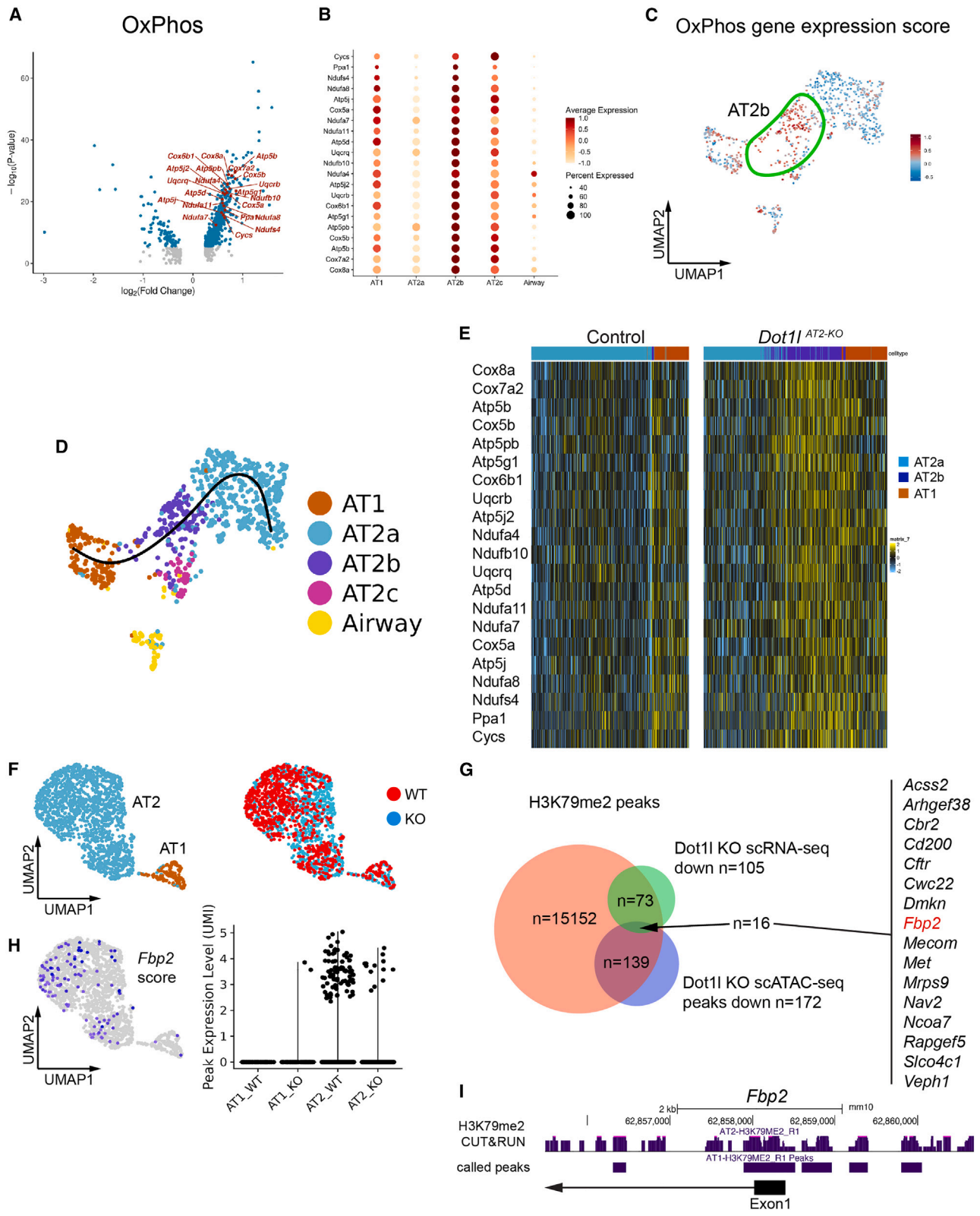

(legend on next page)

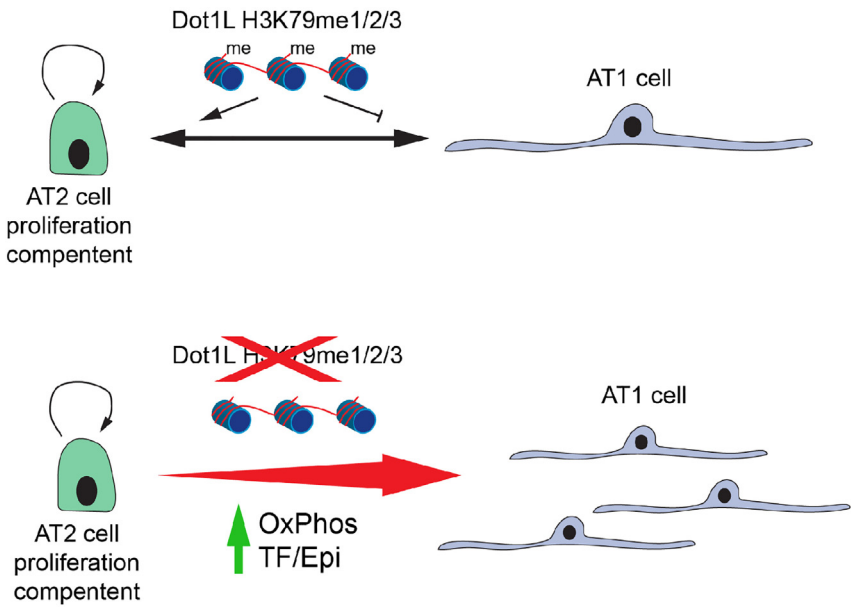

Figure 7. Model of how *Dot1l* regulation of AT2-AT1 differentiation through regulation of OxPhos and a subset of transcription and epigenetic factors

this process could provide better recovery after acute lung injury and open new avenues for pro-regenerative therapies in the lung. We performed an organoid screen and identified DOT1L inhibitors as factors that could promote alveolar growth *ex vivo*. Our data show that loss of *Dot1l* in lung development leads to precocious initiation of the AT1 and AT2 cell fate programs several days prior to their normal activation. In adult models of lung regeneration, our data show that loss of *Dot1l* leads to accelerated AT2-AT1 differentiation with no change in proliferation. This acceleration of AT2-AT1 differentiation is associated with the emergence of a transition AT2 cell population that exhibits enhanced OxPhos metabolism and changes in critical transcription and epigenetic factor gene expression. Thus, *Dot1l* restricts AT2-AT1 differentiation and its inhibition can accelerate this process due in part to enhanced OxPhos metabolism.

Our screen identified pathways that either enhance alveolar growth, such as DOT1L inhibition, or suppress alveolar growth, such as HDAC and BRD4 inhibitors. HDAC pathways have been shown to play key roles in lung epithelial development with *Hdac1/2* required for early airway development (Wang et al., 2013) and *Hdac3* being required for AT1 cell differentiation in late lung development (Wang et al. 2016a, 2016b). The finding that HDAC inhibitors repressed alveolar organoid growth may not be surprising given their well-known ability to inhibit cell proliferation and use as anti-cancer therapies. A role for *Brd4* in lung regeneration has not been reported, although given its ability to epigenetically regulate important pathways in stem cell populations it may play an important role in balancing the self-renewal and differentiation of AT2 cells.

While we observed increased organoid size when AT2 organoids were exposed to DOT1L inhibitors, we did not observe any change in AT2 cell proliferation *in vivo* at homeostasis or after injury. This likely reflects the simplified nature of the organoid assay, which lacks many of the cell types including immune cells that express potent

Figure 6. *Dot1l* suppresses OxPhos gene expression resulting in a unique AT2 cell state correlating with accelerated AT1 differentiation

(A) Volcano plot of OxPhos genes upregulated in the *Dot1l*$^{AT2\text{-}KO}$ mutants.
(B) Dot plot representing a set of highly upregulated OxPhos genes specifically in the AT2b population.
(C) Using genes represented in (A and B) showing the enrichment of OxPhos genes in the AT2b population.
(D) Pseudotime trajectory analysis using Slingshot shows the transcriptional link between AT2a, AT2b, and AT1 cells.
(E) Heatmap of OxPhos gene expression changes revealing the unique increase in OxPhos in the AT2b population that is lacking in the control dataset.
(F) UMAP plot showing scATAC-seq merged data from wild-type and *Dot1l*$^{AT2\text{-}KO}$ mutants at 14 days post-influenza injury.
(G) Venn diagram showing the overlap of genes found with H3K79me2 CUT&RUN marks, downregulated peaks in scATAC-seq data form *Dot1l*$^{AT2\text{-}KO}$ mutants, and downregulated gene expression as measure by scRNA-seq in *Dot1l*$^{AT2\text{-}KO}$ mutants. Circles are not drawn to scale.
(H) *Fbp2* gene score and violin plots of *Fbp2* gene score from scATAC-seq data.
(I) H3K79me2 CUT&RUN tracks for the *Fbp2* gene.

mitogenic cytokines that drive AT2 proliferation after injury such as IL-1b. The precocious activation of AT1 and AT2 cell fate and the increased expression of AT1 and AT2 markers during lung development in *Dot1l*$^{Shh\text{-}KO}$ mutants suggests that the development of these lineages is restricted by the *Dot1l*-regulated epigenetic pathway. Interestingly, this enhanced AT1 and AT2 gene expression normalizes before birth, suggesting a critical temporal response to the effects of *Dot1l* deficiency on lung endoderm development. Deletion of *Dot1l* in mature AT2 cells causes increased AT2-AT1 differentiation after acute lung injury. However, AT2 cell proliferation during the regenerative process after injury was unchanged upon loss of *Dot1l*, indicating that the primary downstream impact of *Dot1l*-mediated transcriptional control is on differentiation. These data suggest that changes in differentiation can be uncoupled from changes in proliferation during lung epithelial regeneration. Similar effects were observed when cell division was blocked in AT2 cells, which did not inhibit activation of the AT1 gene expression program (Liberti et al., 2021). Together, these data suggest that *Dot1l* suppresses alveolar epithelial cell fate commitment during periods of plasticity such as early lung development and regeneration, implicating DOT1l inhibitors as potential candidates for accelerating lung regeneration.

Loss of *Dot1l* led to the emergence of a novel AT2 cell state characterized by elevated OxPhos gene expression and elevated expression of a subset of important transcription and epigenetic factors. The increase in OxPhos gene expression is interesting as it is also associated with differentiation in other cellular systems including T cells (Shin et al., 2020) and stem cells (Mostafavi et al., 2021). While the emergence of an OxPhox metabolic signature could represent the enhanced differentiation of AT1 cells from AT2 cells after loss of *Dot1l*, the increase in OxPhox gene expression observed in the AT2b state was significantly greater than that observed in AT1 cells. Future studies will be critical to provide insight into how metabolic changes alter lung alveolar regeneration.

EXPERIMENTAL PROCEDURES

Resource availability

Corresponding author

Further information and requests for resources and reagents should be directed to and will be fulfilled by the corresponding author Edward E. Morrisey (emorrise@pennmedicine.upenn.edu).

Materials availability

This study did not generate new unique reagents. See details in the following experimental procedures.

Epigenetic inhibitor library screen

The screening was divided into three steps: establishment of AT2 cell organoid cultural system compatible with library screening, library screening, and validation (Sdelci et al., 2016). To set up an alveolar organoid screening platform, we changed our routine 24-well plate with insert cultural system to 96-well plate format without insert. Mouse primary lung fibroblast cells were prepared as described in our previous reports (Frank et al., 2016). FACS sorted AT2 cells (from *Sftpc*^{EGFP} mice JAX no. 028356) (Vanderbilt et al., 2015) were co-cultured with lung mesenchyme for the organoid assays. One thousand AT2 cells and 10,000 mouse primary lung fibroblast cells were suspended in 50 μL of 50% Matrigel in MTEC-SAGM medium, plated in 96-well plates, left to solidify for 15 min at 37°C, and were then covered with 120 μL MTEC-SAGM medium. Forty-eight hours after seeding cells, medium was changed to include 10 μM of one small molecule from the epigenetic library (Selleckchem, L1900) or an equal volume of H_2O or DMSO as negative controls and 50 ng/mL of Fgf7 as a positive control. Medium was changed 9 and 16 days after initial plating with medium containing the 181 epigenetic inhibitors. Nineteen days after the initial addition of the epigenetic library, fluorescence images were acquired with the Evos FL Auto 2 (Invitrogen) using a 4× objective. Total fluorescence intensity of each image was measured using ImageJ program and compared with control (DMSO or H_2O) as a fold of change in comparison with controls. A *Z* score was also measured for the screen using a previously reported algorithm (Zhang 2011).

Validation of DOT1L inhibitors in organoid assays

The three DOT1L inhibitors of DOT1L identified in the initial screen (EPZ004777, EPZ5676, SGC0946) were used to test dose dependency using doses spanning the previously reported optimal concentrations used for each inhibitor (Daigle et al. 2011, 2013; Yu et al., 2012). These dose-dependent assays utilized our previously reported 24-well organoid system (Liberti et al., 2021).

Mouse lines

To generate a *Dot1l* conditional floxed allele, cryopreserved *Dot1l*$^{tm1a(KOMP)}$ embryos from the KOMP Repository-UCDavis (www.komp.org) were reimplanted into surrogate dams to generate the appropriate heterozygous floxed offspring. These mice were bred to the FLPo deleter mouse line (JAX stock no. 012930) to remove the FRT-flanked neomycin resistance cassette. The resulting *Dot1l*$^{flox/+}$ mice were then bred to the previously reported *Shh*^{cre} or *Sftpc*$^{cre/ERT2}$ mice (Harfe et al., 2004; Chapman et al., 2011). All animal experiments were performed under the guidance of the University of Pennsylvania Institutional Animal Care and Use Committee.

Lineage tracing and injury studies

Tamoxifen (Sigma) was dissolved in corn oil with 10% ethanol and *Sftpc*$^{cre/ERT2}$:*Dot1l*$^{flox/flox}$ mice were injected intraperitoneally at a dose of 200 mg/kg body weight for 3 consecutive days, 14 days before mice were injured using H1N1 influenza or hyperoxia treatment. For the influenza injury studies, 2 weeks after tamoxifen induction, PR8 H1N1 influenza (a kind gift from Dr. John Wherry at the University of Pennsylvania) was delivered to anesthetized mice intranasally as reported previously (Liberti et al. 2021). For

hyperoxic lung injury studies, 2 weeks after tamoxifen induction, mice were exposed to 95% oxygen for 3 days as reported previously (Penkala et al., 2021), and allowed to recover at room air for the days indicated in each experiment.

Histology

Embryonic lungs were collected from embryos at the days post conception as indicated and fixed in 2% paraformaldehyde for 24 h. Adult lungs were perfused with PBS via the right ventricle to remove blood, inflated with 2% paraformaldehyde, and allowed to fix overnight. Tissue was processed as described previously (Zepp et al., 2021; Penkala et al., 2021; Liberti et al., 2021). IHC was used to detect protein expression using the following antibodies: Dot1l (rabbit, 1:200, Abcam), H3K79Me2 (rabbit, 1:1,000, Abcam), GFP (chicken, 1:200, Aves, GFP-1020), Sftpc (rabbit, 1:100, Millipore, ABC99), Hopx (mouse, Santa Cruz, sc-514859), Ki67 (mouse, 1:200, Becton Dickenson, 550609), Nkx2.1 (rabbit, 1:50, Santa Cruz), and gama-H2AX (mouse, 1:200, Invitrogen/Fisher). RNAscope was used to detect mRNA expression using the following probes: Mm-Sfpc C1 (Advanced Cell Diagnostics, 314101-C1) and Mm-Hopx C2 Red (Advanced Cell Diagnostics, 405161-C2).

Primer sequences for qPCR

Gene	Forward	Reverse
Gapdh	AAATGGTGAAGGTCGGTGTGAACG	ATCTCCACTTTGCCACTGC
Sftpc	ACCCTGTGTGGAGAGCTACCA	TTTGCGGAGGGTCTTTCCT
Hopx	TTCAACAAGGTCAACAAGCACCCG	CCAGGCGCTGCTTAAACCATTTCT
Aqp5	ATGAACCCAGCCCGATCTTT	ACGATCGGTCCTACCCAGAAG

qPCR analysis

RNA was extracted using QIAGEN RNeasy Kit following the manufacturer's instructions, and was reverse transcribed using Invitrogen SuperScript IV First-Strand Synthesis System (Thermo Scientific, 18091050) SYBR Green I Master MIX and the following primers were used for PCR reactions.

scRNA-seq

At day 14 after influenza infection, lineage-traced (EYFP-positive) cells were collected from five controls and five mutants by FACS isolation, then pooled and processed simultaneously following the recommendations provided by 10X Genomics and as previously reported for scRNA-seq and scATAC-seq analysis (Penkala et al., 2021). In brief, libraries were prepared according to the manufacturer's protocol using Chromium Single Cell 3′ v.3.1 chemistry, and then sequenced on the Illumina NovaSeq 6000 instrument with paired-end 150-bp reads. During data processing, a QC violinplot was made to address differences in data quality between samples and CD31^{+} cells were filtered out. The demultiplexing, barcoded processing, and gene counting were made using STARSolo 2.7.9a, and downstream analysis was performed using Seurat v.4 as we have reported previously (Basil et al., 2022; Zepp et al., 2021; Penkala et al., 2021). Pseudotime trajectory analysis was performed using Slingshot (Street et al., 2018).

scATAC-seq analysis

Cells were isolated as for scRNA-seq and nuclei isolation and counting were conducted according to the manufacturer's protocol (10X Genomics, Single Cell ATAC v.1 reagents). Data processing such as read filtering and alignment, transposase cut site identification, and peak accessibility was conducted using Cell Ranger ATAC pipeline. Data were further processed using the Seurat extension Signac (https://satijalab.org/signac/). Cells were removed if peak fragments were less than 3,000, percent reads in peaks was less than 15%, a genome blocklist ratio was greater than 0.025, and a mono-nucleosomal/nucleosome-free ratio was greater than 10. Normalization was performed using term frequency-inverse document frequency (TF-IDF) and dimension reduction by running singular value decomposition on the TF-IDF normalized matrix. Non-linear reduction was performed similar to scRNA-seq with UMAP and graph-based clustering with the Louvain algorithm. Gene activity score was computed using the chromatin accessibility reads associated with each gene. scATAC-seq and scRNA-seq were integrated using a crossmodality integration and label transfer method to identify shared correlation patterns in the gene activity matrix and scRNA-seq dataset using the FindIntegrationAnchors and IntegrateData functions and Coverageplots were created using Signac.

CUT&RUN analysis

GFP^{+}/Epcam^{+} AT2 cells were FACS sorted from the *Sftpc*^{EGFP} mouse line (Vanderbilt et al., 2015). CUT&RUN was performed (using Cell Signaling, cat. no. 86652) with 200,000 cells/per reaction, and 5 μL Anti-H3K79me2 antibody (Abcam, 3594), 2 μL anti-H3K4me3 (as a positive control), and IgG XP isotype-negative control. DNA was purified using phenol/chloroform extraction followed by ethanol precipitation. DNA libraries were prepared using DNA Library Prep Kit for Illumina. Analysis was performed using the CUT&RUN v.1 Nextflow pipeline from nf-core (https://nf-co.re/cutandrun). In brief, fastq files were adapter trimmed using Trim-galore. Reads were aligned to the mouse reference genome (Grcm38) using Bowtie2 and duplicate reads were marked using Picard. Coverage tracks were created using Bedtools. Peaks were called using SEACR and consensus peaks were called using Bedtools. Plots were created using the UCSC genome browser.

Statistical analysis

qPCR and organoid colony counts used an unpaired t test for measuring statistical significance.

Data access

The genomic data found in this report can be accessed at the GEO under accession no. GSE210800.

Data and code availability

The genomic data found in this report can be accessed at the GEO under accession no. GSE210800.

SUPPLEMENTAL INFORMATION

Supplemental information can be found online at https://doi.org/10.1016/j.stemcr.2023.07.006.

AUTHOR CONTRIBUTIONS

S.L., D.L., J.K., M.C.B., F.L.C.-D., designed and performed organoid and mouse experiments. S.Z. performed histological analysis. M.P.M. performed bioinformatic analysis. S.L. and E.E.M. supervised these studies and co-wrote the manuscript.

ACKNOWLEDGMENTS

The authors wish to thank members of the Morrisey Lab for their helpful comments on this study. This work was supported by funding from the National Institutes of Health (HL162683, HL152194, HL132999, and HL148857) and the BREATH Consortium funded by the Longfonds Society.

CONFLICT OF INTERESTS

The authors declare no competing interests.

Received: January 30, 2023
Revised: July 22, 2023
Accepted: July 23, 2023
Published: August 17, 2023

REFERENCES

Basil, M.C., Cardenas-Diaz, F.L., Kathiriya, J.J., Morley, M.P., Carl, J., Brumwell, A.N., Katzen, J., Slovik, K.J., Babu, A., Zhou, S., et al. (2022). 'Human distal airways contain a multipotent secretory cell that can regenerate alveoli. Nature *604*, 120–126.

Basil, M.C., Katzen, J., Engler, A.E., Guo, M., Herriges, M.J., Kathiriya, J.J., Windmueller, R., Ysasi, A.B., Zacharias, W.J., Chapman, H.A., et al. (2020). The Cellular and Physiological Basis for Lung Repair and Regeneration: Past, Present, and Future. Cell Stem Cell *26*, 482–502.

Chapman, H.A., Li, X., Alexander, J.P., Brumwell, A., Lorizio, W., Tan, K., Sonnenberg, A., Wei, Y., and Vu, T.H. (2011). 'Integrin alpha6beta4 identifies an adult distal lung epithelial population with regenerative potential in mice. J. Clin. Invest. *121*, 2855–2862.

Choi, J., Park, J.E., Tsagkogeorga, G., Yanagita, M., Koo, B.K., Han, N., and Lee, J.H. (2020). 'Inflammatory Signals Induce AT2 Cell-Derived Damage-Associated Transient Progenitors that Mediate Alveolar Regeneration. Cell Stem Cell *27*, 366–382.e7.

Chung, M.I., Bujnis, M., Barkauskas, C.E., Kobayashi, Y., and Hogan, B.L.M. (2018). 'Niche-mediated BMP/SMAD signaling regulates lung alveolar stem cell proliferation and differentiation. Development *145*.

Daigle, S.R., Olhava, E.J., Therkelsen, C.A., Basavapathruni, A., Jin, L., Boriack-Sjodin, P.A., Allain, C.J., Klaus, C.R., Raimondi, A., Scott, M.P., et al. (2013). 'Potent inhibition of DOT1L as treatment of MLL-fusion leukemia. Blood *122*, 1017–1025.

Daigle, S.R., Olhava, E.J., Therkelsen, C.A., Majer, C.R., Sneeringer, C.J., Song, J., Johnston, L.D., Scott, M.P., Smith, J.J., Xiao, Y., et al. (2011). 'Selective killing of mixed lineage leukemia cells by a potent small-molecule DOT1L inhibitor. Cancer Cell *20*, 53–65.

Frank, D.B., Peng, T., Zepp, J.A., Snitow, M., Vincent, T.L., Penkala, I.J., Cui, Z., Herriges, M.J., Morley, M.P., Zhou, S., et al. (2016). 'Emergence of a Wave of Wnt Signaling that Regulates Lung Alveologenesis by Controlling Epithelial Self-Renewal and Differentiation. Cell Rep. *17*, 2312–2325.

Frank, D.B., Penkala, I.J., Zepp, J.A., Sivakumar, A., Linares-Saldana, R., Zacharias, W.J., Stolz, K.G., Pankin, J., Lu, M., Wang, Q., et al. (2019). 'Early lineage specification defines alveolar epithelial ontogeny in the murine lung. Proc. Natl. Acad. Sci. USA *116*, 4362–4371.

Harfe, B.D., Scherz, P.J., Nissim, S., Tian, H., McMahon, A.P., and Tabin, C.J. (2004). 'Evidence for an expansion-based temporal Shh gradient in specifying vertebrate digit identities. Cell *118*, 517–528.

Hu, R., Wang, W.L., Yang, Y.Y., Hu, X.T., Wang, Q.W., Zuo, W.Q., Xu, Y., Feng, Q., and Wang, N.Y. (2022). Identification of a selective BRD4 PROTAC with potent antiproliferative effects in AR-positive prostate cancer based on a dual BET/PLK1 inhibitor. Eur. J. Med. Chem. *227*, 113922.

Huangyang, P., Li, F., Lee, P., Nissim, I., Weljie, A.M., Mancuso, A., Li, B., Keith, B., Yoon, S.S., and Simon, M.C. (2020). 'Fructose-1,6-Bisphosphatase 2 Inhibits Sarcoma Progression by Restraining Mitochondrial Biogenesis. Cell Metabol. *31*, 1032–1188.e7.

Kobayashi, Y., Tata, A., Konkimalla, A., Katsura, H., Lee, R.F., Ou, J., Banovich, N.E., Kropski, J.A., and Tata, P.R. (2020). 'Persistence of a regeneration-associated, transitional alveolar epithelial cell state in pulmonary fibrosis. Nat. Cell Biol. *22*, 934–946.

Leach, J.P., and Morrisey, E.E. (2018). Repairing the lungs one breath at a time: How dedicated or facultative are you? Genes Dev. *32*, 1461–1471.

Li, J., Wang, Z., Chu, Q., Jiang, K., Li, J., and Tang, N. (2018). 'The Strength of Mechanical Forces Determines the Differentiation of Alveolar Epithelial Cells. Dev. Cell *44*, 297–312.e5.

Liberti, D.C., Kremp, M.M., Liberti, W.A., 3rd, Penkala, I.J., Li, S., Zhou, S., and Morrisey, E.E. (2021). 'Alveolar epithelial cell fate is maintained in a spatially restricted manner to promote lung regeneration after acute injury. Cell Rep. *35*, 109092.

Liberti, D.C., Liberti Iii, W.A., Kremp, M.M., Penkala, I.J., Cardenas-Diaz, F.L., Morley, M.P., Babu, A., Zhou, S., Fernandez Iii, R.J., and Morrisey, E.E. (2022). 'Klf5 defines alveolar epithelial type 1 cell lineage commitment during lung development and regeneration. Dev. Cell *57*, 1742–1757.e5.

Liberti, D.C., Zepp, J.A., Bartoni, C.A., Liberti, K.H., Zhou, S., Lu, M., Morley, M.P., and Morrisey, E.E. (2019). 'Dnmt1 is required for proximal-distal patterning of the lung endoderm and for restraining alveolar type 2 cell fate. Dev. Biol. *454*, 108–117.

Mostafavi, S., Balafkan, N., Pettersen, I.K.N., Nido, G.S., Siller, R., Tzoulis, C., Sullivan, G.J., and Bindoff, L.A. (2021). 'Distinct Mitochondrial Remodeling During Mesoderm Differentiation in a Human-Based Stem Cell Model. Front. Cell Dev. Biol. *9*, 744777.

Nabhan, A.N., Brownfield, D.G., Harbury, P.B., Krasnow, M.A., and Desai, T.J. (2018). 'Single-cell Wnt signaling niches maintain stemness of alveolar type 2 cells. Science *359*, 1118–1123.

Nishiyama, A., Dey, A., Miyazaki, J.I., and Ozato, K. (2006). 'Brd4 is required for recovery from antimicrotubule drug-induced mitotic arrest: preservation of acetylated chromatin. Mol. Biol. Cell *17*, 814–823.

Osipova, E., Barsacchi, R., Brown, T., Sadanandan, K., Gaede, A.H., Monte, A., Jarrells, J., Moebius, C., Pippel, M., Altshuler, D.L., et al. (2023). 'Loss of a gluconeogenic muscle enzyme contributed to adaptive metabolic traits in hummingbirds. Science *379*, 185–190.

Pang, Y., Bai, G., Zhao, J., Wei, X., Li, R., Li, J., Hu, S., Peng, L., Liu, P., and Mao, H. (2022). The BRD4 inhibitor JQ1 suppresses tumor

growth by reducing c-Myc expression in endometrial cancer. J. Transl. Med. *20*, 336.

Penkala, I.J., Liberti, D.C., Pankin, J., Sivakumar, A., Kremp, M.M., Jayachandran, S., Katzen, J., Leach, J.P., Windmueller, R., Stolz, K., et al. (2021). 'Age-dependent alveolar epithelial plasticity orchestrates lung homeostasis and regeneration. Cell Stem Cell *28*, 1775–1789.e5.

Sdelci, S., Lardeau, C.H., Tallant, C., Klepsch, F., Klaiber, B., Bennett, J., Rathert, P., Schuster, M., Penz, T., Fedorov, O., et al. (2016). 'Mapping the chemical chromatin reactivation landscape identifies BRD4-TAF1 cross-talk. Nat. Chem. Biol. *12*, 504–510.

Shin, B., Benavides, G.A., Geng, J., Koralov, S.B., Hu, H., Darley-Usmar, V.M., and Harrington, L.E. (2020). Mitochondrial Oxidative Phosphorylation Regulates the Fate Decision between Pathogenic Th17 and Regulatory T Cells. Cell Rep. *30*, 1898–1909.e4.

Street, K., Risso, D., Fletcher, R.B., Das, D., Ngai, J., Yosef, N., Purdom, E., and Dudoit, S. (2018). 'Slingshot: cell lineage and pseudotime inference for single-cell transcriptomics. BMC Genom. *19*, 477.

Strunz, M., Simon, L.M., Ansari, M., Kathiriya, J.J., Angelidis, I., Mayr, C.H., Tsidiridis, G., Lange, M., Mattner, L.F., Yee, M., et al. (2020). 'Alveolar regeneration through a Krt8+ transitional stem cell state that persists in human lung fibrosis. Nat. Commun. *11*, 3559.

Sun, S., Zhao, W., Li, Y., Chi, Z., Fang, X., Wang, Q., Han, Z., and Luan, Y. (2021). 'Design, synthesis and antitumor activity evaluation of novel HDAC inhibitors with tetrahydrobenzothiazole as the skeleton. Bioorg. Chem. *108*, 104652.

Vanderbilt, J.N., Gonzalez, R.F., Allen, L., Gillespie, A., Leaffer, D., Dean, W.B., Chapin, C., and Dobbs, L.G. (2015). 'High-efficiency type II cell-enhanced green fluorescent protein expression facilitates cellular identification, tracking, and isolation. Am. J. Respir. Cell Mol. Biol. *53*, 14–21.

Wang, X., Wang, Y., Snitow, M.E., Stewart, K.M., Li, S., Lu, M., and Morrisey, E.E. (2016a). 'Expression of histone deacetylase 3 instructs alveolar type I cell differentiation by regulating a Wnt signaling niche in the lung. Dev. Biol. *414*, 161–169.

Wang, Y., Frank, D.B., Morley, M.P., Zhou, S., Wang, X., Lu, M.M., Lazar, M.A., and Morrisey, E.E. (2016b). 'HDAC3-Dependent Epigenetic Pathway Controls Lung Alveolar Epithelial Cell Remodeling and Spreading via miR-17-92 and TGF-beta Signaling Regulation. Dev. Cell *36*, 303–315.

Wang, Y., Tian, Y., Morley, M.P., Lu, M.M., Demayo, F.J., Olson, E.N., and Morrisey, E.E. (2013). 'Development and regeneration of Sox2+ endoderm progenitors are regulated by a Hdac1/2-Bmp4/Rb1 regulatory pathway. Dev. Cell *24*, 345–358.

Wood, K., Tellier, M., and Murphy, S. (2018). DOT1L and H3K79 Methylation in Transcription and Genomic Stability. Biomolecules *8*.

Xiang, T., Bai, J.Y., She, C., Yu, D.J., Zhou, X.Z., and Zhao, T.L. (2018). 'Bromodomain protein BRD4 promotes cell proliferation in skin squamous cell carcinoma. Cell. Signal. *42*, 106–113.

Yin, Z., Gonzales, L., Kolla, V., Rath, N., Zhang, Y., Lu, M.M., Kimura, S., Ballard, P.L., Beers, M.F., Epstein, J.A., and Morrisey, E.E. (2006). 'Hop functions downstream of Nkx2.1 and GATA6 to mediate HDAC-dependent negative regulation of pulmonary gene expression. Am. J. Physiol. Lung Cell Mol. Physiol. *291*, L191–L199.

Yu, W., Chory, E.J., Wernimont, A.K., Tempel, W., Scopton, A., Federation, A., Marineau, J.J., Qi, J., Barsyte-Lovejoy, D., Yi, J., et al. (2012). Catalytic site remodelling of the DOT1L methyltransferase by selective inhibitors. Nat. Commun. *3*, 1288.

Zacharias, W.J., Frank, D.B., Zepp, J.A., Morley, M.P., Alkhaleel, F.A., Kong, J., Zhou, S., Cantu, E., and Morrisey, E.E. (2018). 'Regeneration of the lung alveolus by an evolutionarily conserved epithelial progenitor. Nature *555*, 251–255.

Zepp, J.A., Morley, M.P., Loebel, C., Kremp, M.M., Chaudhry, F.N., Basil, M.C., Leach, J.P., Liberti, D.C., Niethamer, T.K., Ying, Y., et al. (2021). 'Genomic, epigenomic, and biophysical cues controlling the emergence of the lung alveolus. Science *371*.

Zepp, J.A., and Morrisey, E.E. (2019). 'Cellular crosstalk in the development and regeneration of the respiratory system. Nat. Rev. Mol. Cell Biol. *20*, 551–566.

Zhang, X.D. (2011). 'Illustration of SSMD, z score, SSMD*, z* score, and t statistic for hit selection in RNAi high-throughput screens. J. Biomol. Screen *16*, 775–785.

Zhu, X., Leboeuf, M., Liu, F., Grachtchouk, M., Seykora, J.T., Morrisey, E.E., Dlugosz, A.A., and Millar, S.E. (2022). 'HDAC1/2 Control Proliferation and Survival in Adult Epidermis and PreBasal Cell Carcinoma through p16 and p53. J. Invest. Dermatol. *142*, 77–87.e10.